SOFAR Float Observations of an Intermediate-Depth Eastern Boundary Current and Mesoscale Variability in the Eastern Tropical Atlantic Ocean*

DAVID M. FRATANTONI AND PHILIP L. RICHARDSON

Department of Physical Oceanography, Woods Hole Oceanographic Institution, Woods Hole, Massachusetts

(Manuscript received 28 August 1997, in final form 13 July 1998)

ABSTRACT

Two neutrally buoyant SOFAR floats vigorously looped and meandered at depths of 950–1150 m in the eastern tropical Atlantic Ocean. The float trajectories illustrate a poleward flow along the tropical eastern boundary and significant intermediate-depth mesoscale variability in the low-latitude eastern basin. One float, caught within an energetic cyclonic eddy near the eastern boundary, looped cyclonically 14 times while translating 600 km northward parallel to the African coastline. A second float, launched near the Mid-Atlantic Ridge, meandered eastward with a Lagrangian zonal wavelength of 400 km and meridional amplitude exceeding 200 km. Satellite infrared imagery indicates that horizontal shear associated with the system of near-surface zonal equatorial currents may contribute to the observed intermediate-depth variability.

1. Introduction

Between January and February 1989 48 neutrally buoyant SOFAR floats were deployed at 800, 1800, and 3300 dbar in the tropical Atlantic Ocean. Most of these floats were launched in the western tropical Atlantic near the coast of South America. Their trajectories described the southward deep western boundary current, the swirl and translation characteristics of North Brazil Current rings, reversing flows along the equator, and deep off-equatorial jets (see Richardson et al. 1992, 1994a, 1994b; Richardson and Schmitz 1993; Richardson and Fratantoni 1999). Three of the 800-dbar floats were launched east of the Mid-Atlantic Ridge along 11°N. The trajectories of two floats revealed a complex combination of wavelike meandering, persistent looping, and rapid translation in the low-latitude eastern Atlantic (Fig. 1). In this study, these meandering and looping float trajectories are examined and the characteristics and origins of the mesoscale features they illustrate are investigated.

The remainder of this article is organized as follows. In section 2, the acquisition and processing of the SOFAR float data is described. The float trajectories are discussed in detail in section 3. In sections 4 and 5, the large-scale circulation patterns implied by the float trajectories are discussed, and characteristics of the observed intermediate-depth wave and eddy motions are derived. Satellite infrared imagery is used in section 6 to investigate the physical processes responsible for the observed float behavior. Our conclusions are presented in section 7.

2. Data and methods

SOFAR floats periodically emit a low-frequency acoustic pulse that is received and recorded by an array of moored listening stations. The difference in pulse arrival time at each of several listening stations is used to triangulate float position. The floats discussed herein transmitted an 80-s, 250-Hz acoustic signal once per day to an array of listening stations moored in the central and western tropical Atlantic and in a region west of the Canary Islands (Fig. 1). The raw acoustic time-of-arrival data were converted to geographic positions, float velocities were calculated, and quality control procedures were applied. Details of the listening station array and float tracking and processing procedures have been given by Richardson et al. (1994a). The average accuracy of a float position was estimated to be less than 10 km based on a comparison of float launch locations and initial tracking fixes.

Due to a software error the floats failed to correctly transmit the in situ temperature and pressure measurements normally encoded within their acoustic broadcasts. The floats also failed to activate their buoyancy control systems. Without active ballasting a float grad-

* Woods Hole Oceanographic Institution Contribution Number 9691.

Corresponding author address: Dr. David M. Fratantoni, Department of Physical Oceanography, Woods Hole Oceanographic Institution, Woods Hole, MA 02543.
E-mail: dfratantoni@whoi.edu

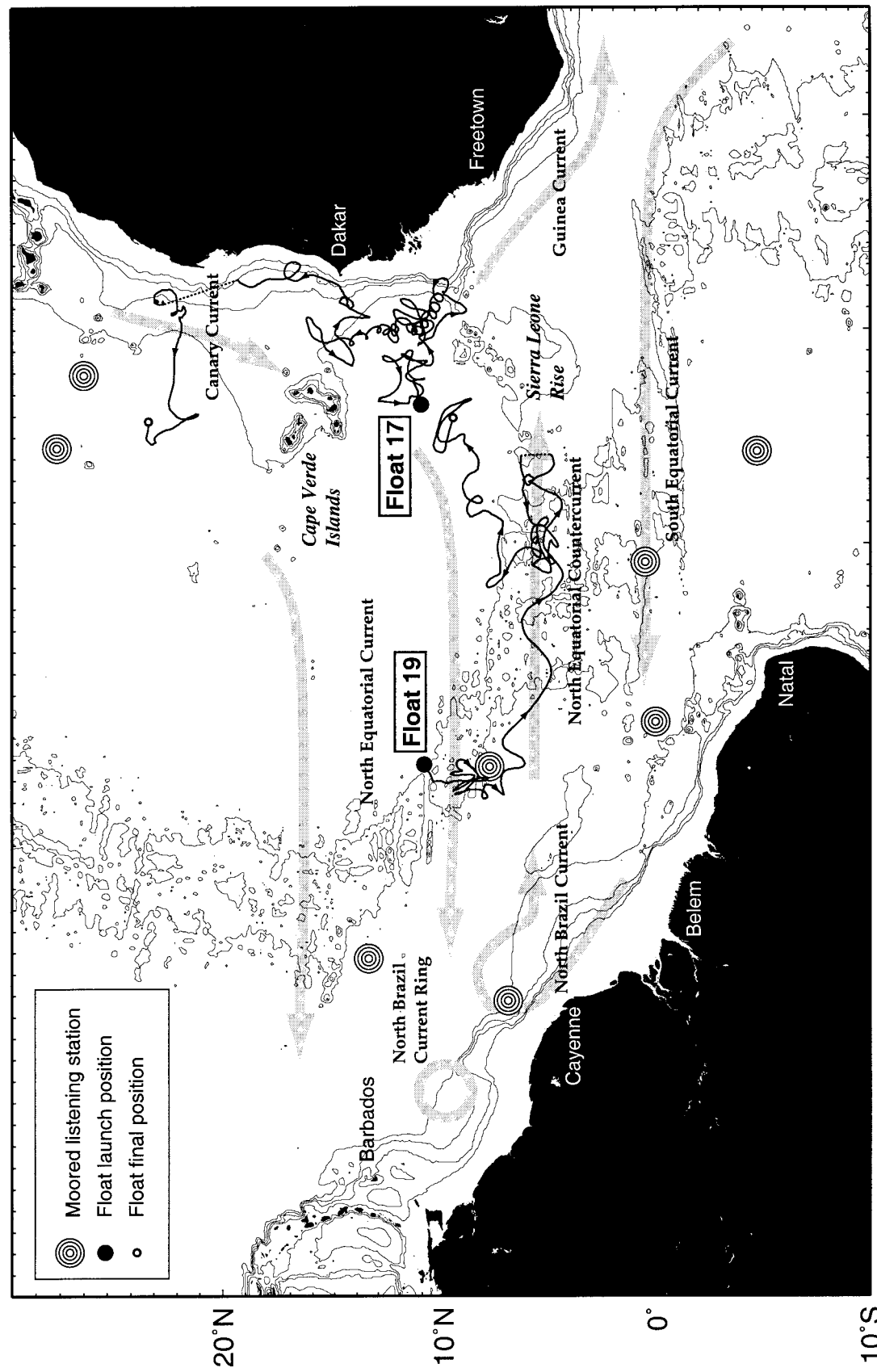

FIG. 1. Trajectories of tropical Atlantic SOFAR floats 17 and 19. The locations of autonomous listening station moorings that recorded acoustic transmissions from the SOFAR floats are also shown. Float trajectory segments during which acoustic tracking was not possible are indicated by dashed lines. Bathymetry is shown with a contour interval of 1000 m. Major surface currents are shown schematically, based on the ship-drift climatologies of Richardson and Walsh (1986) and Mariano et al. (1995).

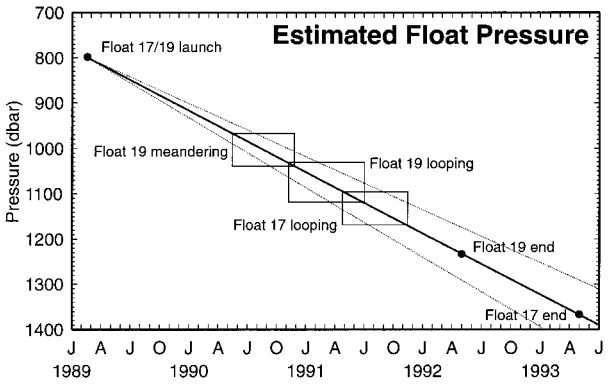

FIG. 2. Estimated pressure in dbar of floats 17 and 19 as a function of time (solid line). Dashed lines indicate an uncertainty estimate corresponding to one standard error of the float sink rate. A mean sink rate of 0.37 ± 0.05 dbar/day was determined by Richardson et al. (1994a) for a sample of 10 aluminum-hulled floats similar to floats 17 and 19. The periods of float looping and meandering are indicated for reference. The uncertainty in the initial float depth is estimated to be approximately 50 dbar based on earlier experiments.

ually sinks due to slow deformation of its pressure housing. Historical SOFAR float data suggest that over the 4.1-yr period during which float 17 was acoustically tracked, it sank from an initial pressure of 800 dbar to approximately 1350 ± 75 dbar (Fig. 2). Float 19 was tracked for a somewhat shorter period (3.2 yrs) and sank to an estimated pressure of 1235 dbar.

The depth range through which the floats descended is just beneath the local minimum in salinity associated with Antarctic Intermediate Water. Archived regional hydrographic observations indicate that salinity increases by about 0.1 between 800 and 1300 m (mean value 34.83), while temperature decreases by less than 1°C (mean value 5.2°C). While we cannot discount the possibility that the float trajectories were influenced by vertically inhomogeneous flows, the available hydrographic evidence suggests that the floats remained within a layer of relatively constant temperature and salinity characteristics.

3. Description of float trajectories

a. Float 17

Float 17 was deployed in February 1989 midway between the Cape Verde Islands and the Sierra Leone Rise (Fig. 1; Table 1). The 51-month 10 300-km trajectory of this float indicates that the character and intensity of flow near the eastern boundary varies significantly in time and space (Fig. 3). This is also evident in a time series of float velocity (Fig. 4) that highlights particularly strong oscillatory velocities during a 5-month period of cyclonic looping in 1991.

During the first 26 months following deployment (February 1989–April 1991) float 17 slowly drifted eastward at a mean speed of 0.8 cm s^{-1} (Fig. 3). As it approached the continental margin near 10°N, the float began looping within a cyclonic eddy. Float 17 looped within this eddy 14.3 times over the next 5 months while translating 600 km toward 335° at a mean speed of 4.1 cm s^{-1}. Based on the estimated sink rate (Fig. 2) the float depth during this looping segment was 1100–1150 dbar. Between November 1991 and June 1992 the float again drifted eastward at a slow 1.3 cm s^{-1}. Upon reaching the 2000-m isobath west of Dakar, float 17 drifted rapidly northward at 8.2 cm s^{-1} along a trajectory parallel to and within 150 km of the eastern boundary until finally, in November 1992, the float drifted westward into the interior near 22°N. Acoustic tracking was lost for a period of about two months in the fall of 1992 (see dashed segment in Fig. 3b). Float 17 was still heard by the array of moored listening stations at the time they were recovered in May 1993.

b. Float 19

Float 19 was launched near 11°N just east of the axis of the Mid-Atlantic Ridge (Fig. 1; Table 1). After launch and prior to June 1990 the float drifted slowly southward across the ridge to about 8°N with a mean speed of 1.3 cm s^{-1} (Fig. 5). It then moved rapidly eastward in a meandering path with meridional displacements greater than 200 km. The average speed during this period was 10.8 cm s^{-1}, and for a short period in July 1990 the eastward float velocity exceeded 25 cm s^{-1} (Fig. 6). Acoustic tracking was interrupted for approximately 18 days between 24 October and 12 November 1990. During this period, float 19 turned cyclonically toward the west. Over the next seven months the float looped cyclonically six times while intermittently translating westward (for 3 loops), eastward (1 loop), and then westward again (2 loops). The float stopped looping at the end of June 1991, moved rapidly northwestward to 8°N, and finally wandered off to the northeast at 3.3 cm s^{-1}. Float 19 was heard by the moored listening stations until mid-May 1992.

TABLE 1. Initial and final position data for floats 17 and 19. Float 17 was still heard by the autonomous listening stations at the time they were recovered (May 1993).

Float	Initial position			Final position			Days tracked
	Date	Lat	Long	Date	Lat	Long	
TA 17	890217	11.22°N	23.18°W	930520	23.28°N	24.28°W	1496
TA 19	890211	11.11°N	40.36°W	920517	09.57°N	24.22°W	1174

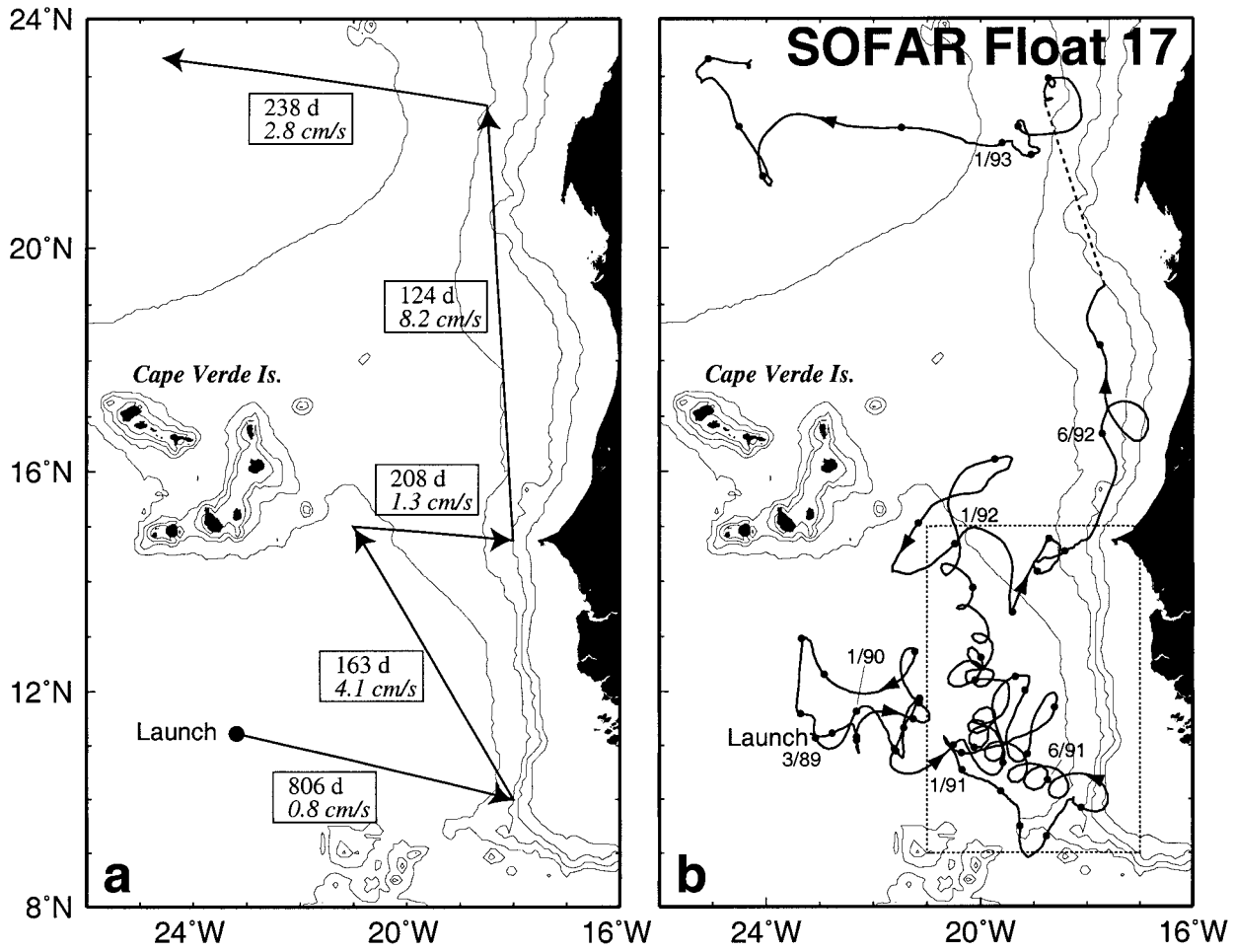

FIG. 3. (a) The trajectory of float 17 subdivided into five segments of different dynamical character. (b) The complete trajectory of float 17. Solid dots are spaced at one-month intervals. Missing data is indicated by a dashed line. Bathymetry is shown with a contour interval of 1000 m. The dashed box indicates the subregion of intense cyclonic looping examined in section 4 (see Fig. 7).

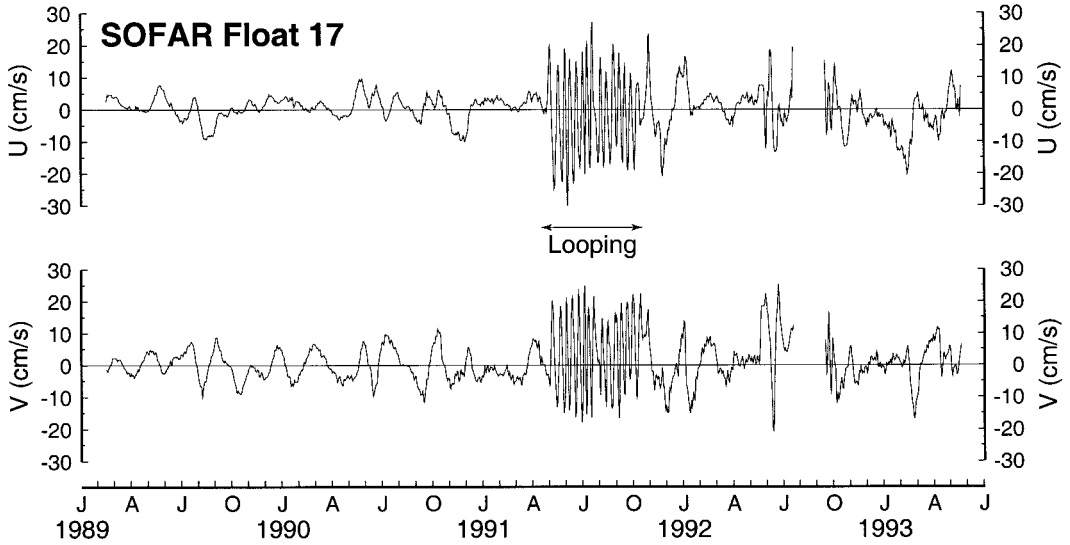

FIG. 4. East (U) and north (V) velocity as measured by float 17. The period of intense cyclonic looping is indicated.

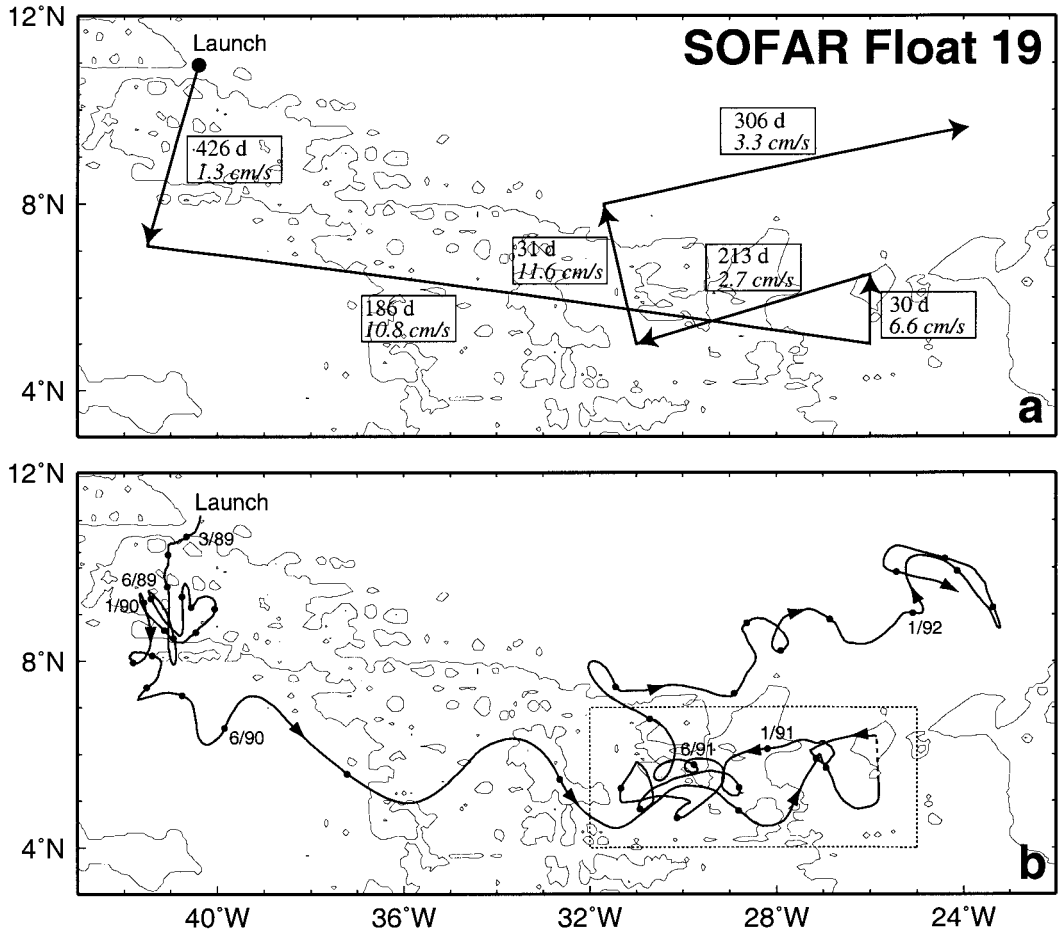

FIG. 5. (a) The trajectory of float 19 subdivided into six segments of generally distinct dynamical character. (b) The complete trajectory of float 19. Missing data is indicated by a dashed line. Solid dots are spaced at one-month intervals. The dashed box indicates the subregion of cyclonic looping examined in section 4 (see Fig. 10).

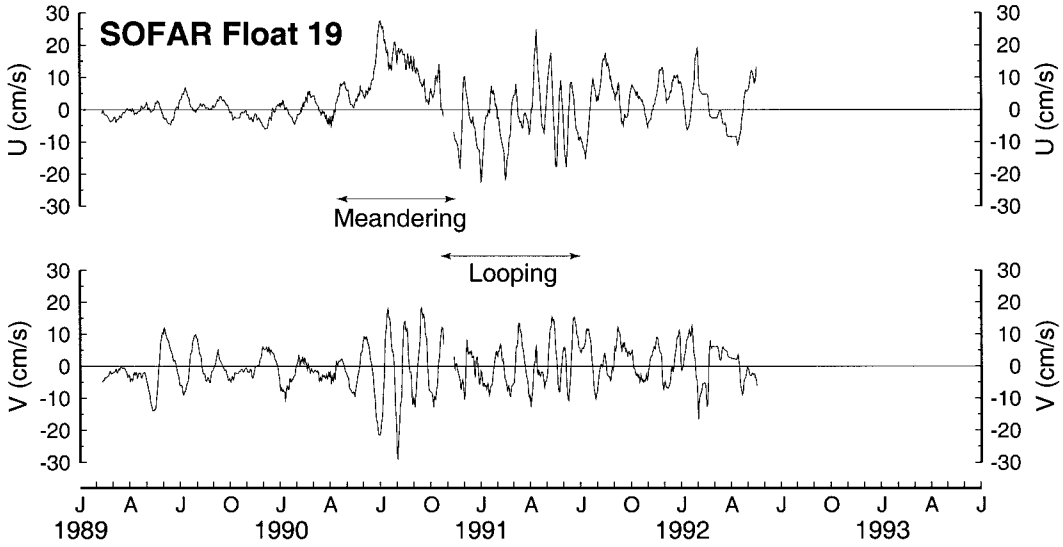

FIG. 6. East (U) and north (V) velocity as measured by float 19. The periods of meandering and cyclonic looping are indicated.

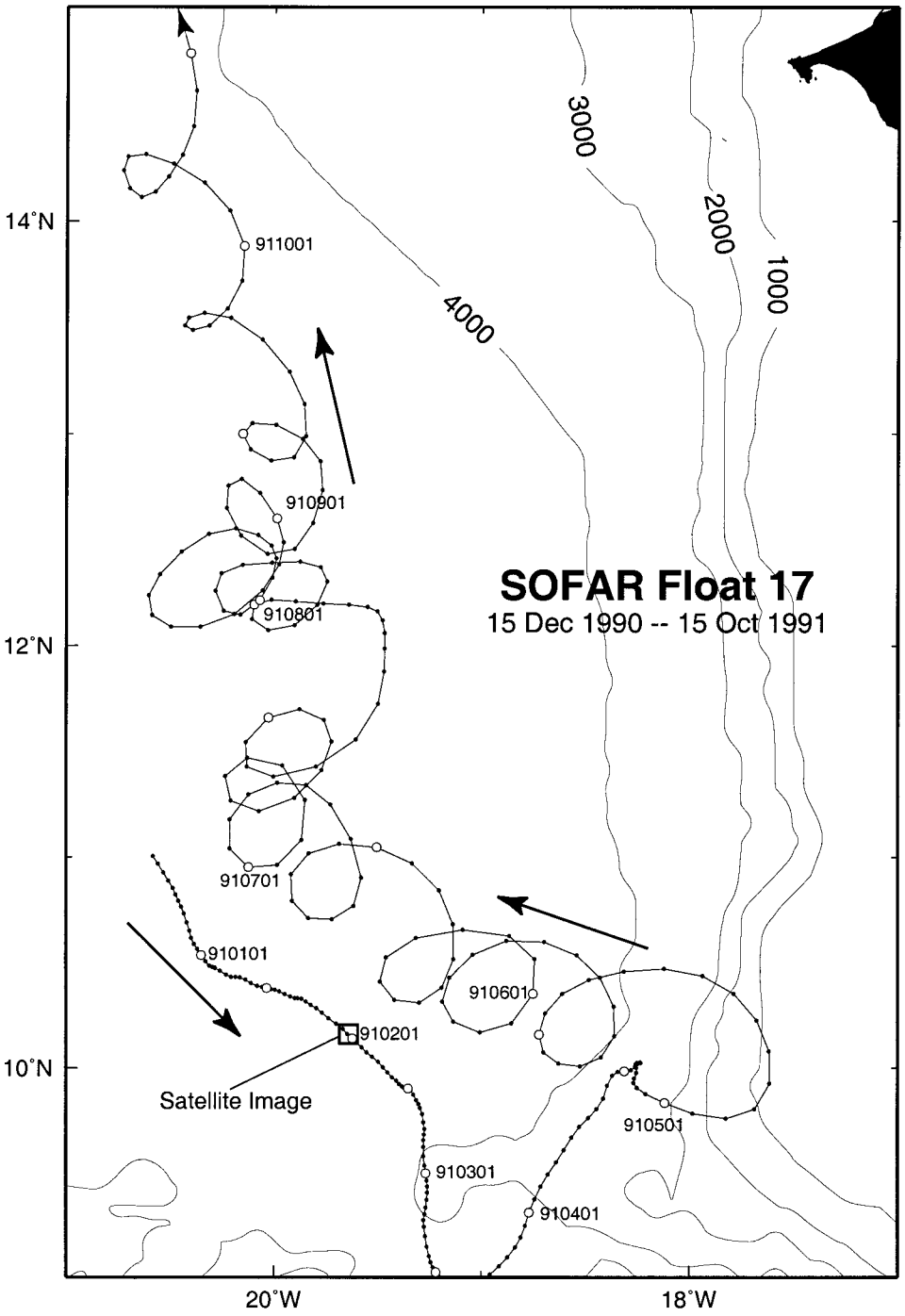

FIG. 7. Detail of float 17 during its intense cyclonic looping. The loops are largest and nearly circular when eddy translation is slow, and smaller and more cusplike when translation is rapid. Solid dots are spaced once per day, and open circles are placed on the 1st and 15th of each month. Bathymetry is shown with a contour interval of 1000 m. The location of float 17 at the time of the satellite image shown in Fig. 13 is indicated.

4. Large-scale circulation patterns

The overall circulation pattern illustrated by floats 17 and 19 is that of flow toward the eastern boundary south of the Cape Verde Islands, flow northward along the boundary between 14° and 22°N, and flow westward into the subtropical gyre interior at 22°–24°N (Fig. 1). It is not evident whether the northward flow along the eastern boundary is related to the local or gyre-scale

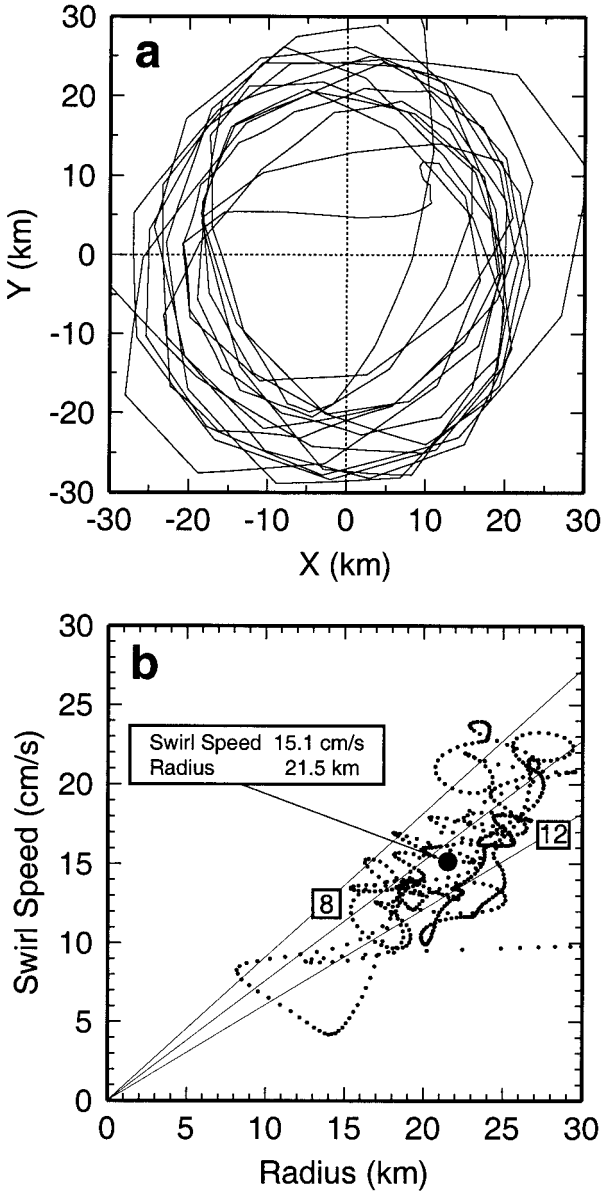

FIG. 8. (a) Residual rotational component of float 17 position (in kilometers relative to the eddy center) after the low-frequency translational component was removed by application of a low-pass Gaussian-shaped filter. (b) Scatterplot of swirl speed (defined as rms velocity about the low-passed velocity) versus radial distance from the eddy center. The general positive correlation suggests an eddy in solid-body rotation. Straight lines indicate slope corresponding to a solid-body rotation period of 8, 10, and 12 days. The mean swirl speed and radius are identified.

wind forcing or is, instead, a component of a different circulation system. The float trajectories are consistent with our understanding of the regional upper-ocean wind-driven circulation with the important exception that hydrographic measurements (Reid 1994), surface drifters (Richardson 1984), ship drifts (Richardson and Walsh 1986), and consideration of Sverdrup transport patterns (Mayer and Weisberg 1993) all indicate *southward* upper-ocean flow along the eastern boundary.

In the annual mean, the North Equatorial Current (NEC) flows westward north of 10°N, while the North Equatorial Countercurrent (NECC) and Guinea Current flow eastward south of this latitude. These currents are generally surface intensified, with the strongest velocities at depths shallower than the 100–200-m tropical thermocline (e.g., Düing et al. 1980; Garzoli and Katz 1983). Near the African coast, observations of poleward eastern boundary currents between 10° and 20°N have been summarized by Barton (1989). None of these observations indicate strong northward flow close to the boundary in the 1000–1300-m depth range. In contrast, one of our floats (float 17) illustrates the (at least temporary) existence of a poleward boundary current at these depths extending from 14° to 22°N. The possible existence of an eastern boundary connection between the equatorial and subtropical Atlantic is particularly relevant to the Atlantic meridional overturning cell.

This overturning circulation (e.g., Schmitz 1995) is forced by high-latitude deep-water formation and requires a northward return flow of surface and intermediate water at all latitudes in the Atlantic to compensate for a net southward export of deep water. Most of the return flow through the tropical Atlantic has been assumed to occur in the western boundary layer (Schmitz 1995; Fratantoni 1996) with additional contributions from mesoscale North Brazil Current rings (Fratantoni et al. 1995) and interior Ekman and geostrophic transport (Mayer and Weisberg 1993). The combined trajectories of floats 17 and 19 suggest that intergyre transport of intermediate water at depths near 1000 m may also occur along the eastern boundary. The components of such a transport pathway would include cross-equatorial western boundary flow in the North Brazil Current, eastward flow beneath the North Equatorial Countercurrent, and northward flow across the equatorial–tropical gyre boundary in a subsurface eastern boundary current. The float trajectories provide evidence for the existence of such a pathway, but the data

TABLE 2. Distance and velocity data for floats 17 and 19. Distance traveled is reported both as a net displacement (initial to final position) and as a pathlength integrated along the float trajectory.

	Distance traveled (km)		Rms velocity (cm s^{-1})		Average velocity (cm s^{-1})	
Float	Displacement	Pathlength	North	East	North	East
TA 17	1300	10300	6.8	6.6	0.8	0.0
TA 19	1800	8800	6.7	7.8	−0.3	1.8

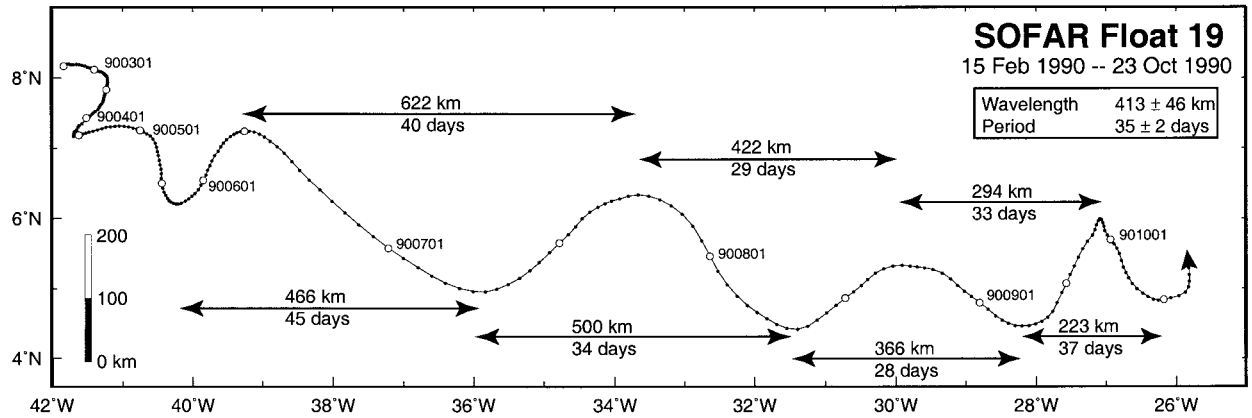

FIG. 9. Detail of float 19 during the period of fast eastward motion and energetic meandering. Crest-to-crest measurements of Lagrangian wavelength and period are shown. A scale for determining meridional amplitude (in kilometers) appears in the lower left-hand corner. Solid dots are spaced once per day, and open circles are placed on the 1st and 15th of each month.

do not allow estimation of its magnitude or relative importance.

5. Intermediate-depth eddies and meanders

Both floats meander and loop. The degree of ''loopiness'' is evident by comparing the float-lifetime displacement to the actual alongpath distance traveled (Table 2). For example, the length of the float 17 trajectory is nearly 8 times the straight-line displacement between initial and final positions. The difference between mean and rms float velocities is also indicative of energetic eddies and meanders superimposed on a relatively slow background flow. In this section we examine more closely the characteristics of these observed modes of variability.

a. Float 17: An intense cyclonic eddy

During a five-month period between April and October 1991, float 17 completed 14.3 cyclonic loops around an eddy of unknown origin (Fig. 7). The looping began between 15 and 20 April following a 2-month excursion southward to 9°N and then back to 10°N. The trajectory of float 17 provides quantitative information about the period of rotation, swirl speed, and translation rate of the observed eddy. To extract this information, time series of float position and velocity were smoothed

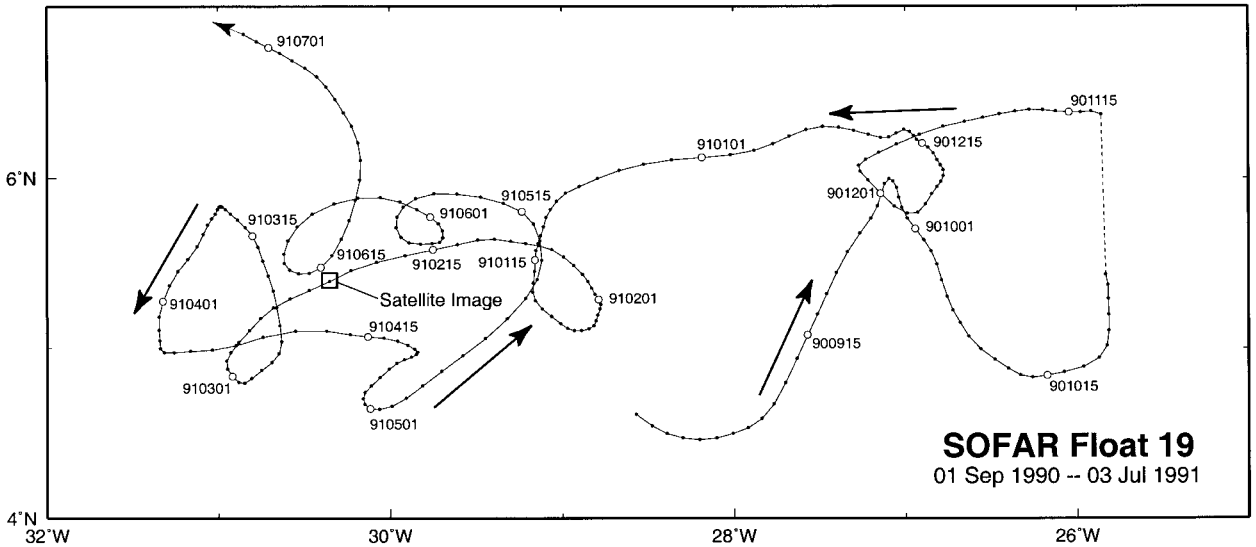

FIG. 10. Detail of float 19 during the period of cyclonic looping. The first three loops are consistent with an eddy translating toward the west at about 4 cm s^{-1}. These loops correspond to a rotation period between 13–23 days and were 15–25 km in radius. A large (50 radius km) cyclonic loop occurred while the float trajectory reversed direction from west to east in April 1991. Solid dots are spaced once per day, and open circles are placed on the 1st and 15th of each month. The location of float 19 at the time of the satellite image shown in Fig. 11 is indicated.

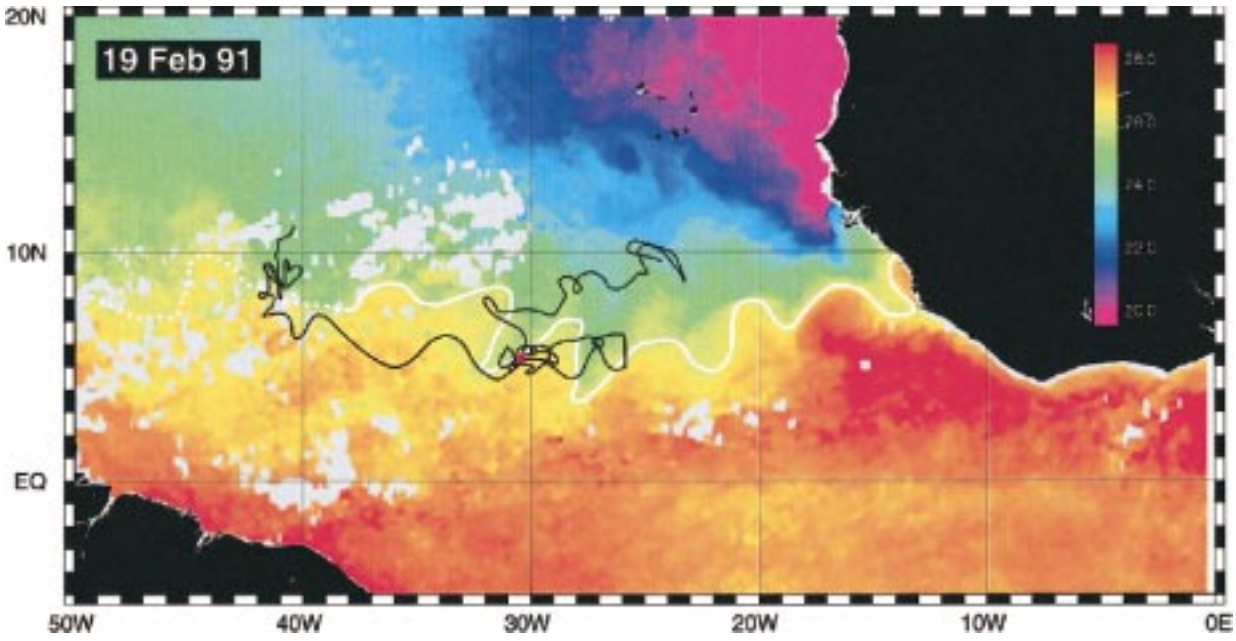

FIG. 11. Fourteen-day composite sea surface temperature image centered on 19 February 1991. Warmer temperatures are red, cooler temperatures are blue. Areas of missing data are shaded gray. The color palette was designed to provide maximum contrast in the 5°–10° N region of interest. The longer and lower-latitude tropical instability waves (found near ±5° latitude; e.g., Steger and Carton 1991) are not readily visible. The complete trajectory of float 19 is shown by the black line. Note that due to the extreme cloud cover during boreal summer, SST images were not available during the meandering portion of the float trajectory. The location of the float on the date corresponding to the image is indicated by the red dot. A smoothed representation of the 26°C isotherm is depicted by the white contour.

with a Gaussian-shaped low-pass filter with an *e*-folding scale of 45 days, approximately four times the mean rotation period. The rotational component of the eddy velocity and the radius of the float from the eddy center were obtained by subtracting the filtered time series from the original series. The average eddy translation speed between 15 April and 15 October was 4.1 cm s^{-1}. Translation was most rapid near the end of the looping period (October) and slowest during August when the eddy appeared to stall near 12°N.

The rotational component of the float trajectory is shown in Fig. 8a. The average looping radius was 21.5 km and varied from 15 to 30 km. Swirl speed, defined as the root mean square of the observed velocity about the low-passed velocity, is plotted as a function of radius in Fig. 8b for each daily velocity observation. The mean swirl speed was 15.1 cm s^{-1}. The period of eddy rotation varied between about 8 and 14 days with a mean near 10 days. While there is some scatter, a general positive correlation of swirl speed with radius indicates an eddy core in approximate solid-body rotation. The maximum observed radius (30 km) is not necessarily the true radius of maximum velocity (the float did not sample all radii within the eddy) but is useful as a lower bound. The overall eddy size is probably larger than 30 km. As a point of comparison, Spall (1992) determined the deformation radii associated with the first two baroclinic modes in this region to be 57 and 29 km. Were this cyclonic eddy the deep manifestation of a surface feature, one might expect a horizontal scale comparable to the first baroclinic Rossby radius. We computed the vertical structure of the first three baroclinic modes from archived regional hydrographic observations. The zero-crossing in the first baroclinic mode occurs at approximately 1400 m. The modal amplitude at 1100 m is about 25% of the value in the upper thermocline, suggesting a relatively intense surface signature.

A useful discriminant between coherent closed eddies and less robust features is the beta Rossby number R_β defined as $U/\beta L^2$, where U and L are typical values of swirl speed and eddy radius (L. Pratt 1998, personal communication). Here $R_\beta \ll 1$ implies that an eddy will rapidly break up into Rossby waves because the local potential vorticity gradient is dominated by the planetary vorticity gradient (β) rather than the eddy's relative vorticity. For U and L of 20 cm s^{-1} and 50 km R_β is $O(1)$, indicating that the observed eddy is capable of trapping and transporting fluid within its core. This characteristic is relevant to the role of such eddies as an intergyre property transport mechanism.

For an eddy in solid-body rotation, a Rossby number based on the ratio of relative vorticity ζ to planetary vorticity f can be determined. Taking ζ equal to twice the rate of eddy rotation yields a Rossby number $\overline{R}_o = \zeta/f$ of 0.07–0.09 for a latitude range of 10°–14°N. Small $\overline{R}_o$ indicates that the momentum balance within the eddy is primarily geostrophic. Although not particularly nonlinear relative to cyclonic Gulf Stream rings, which have

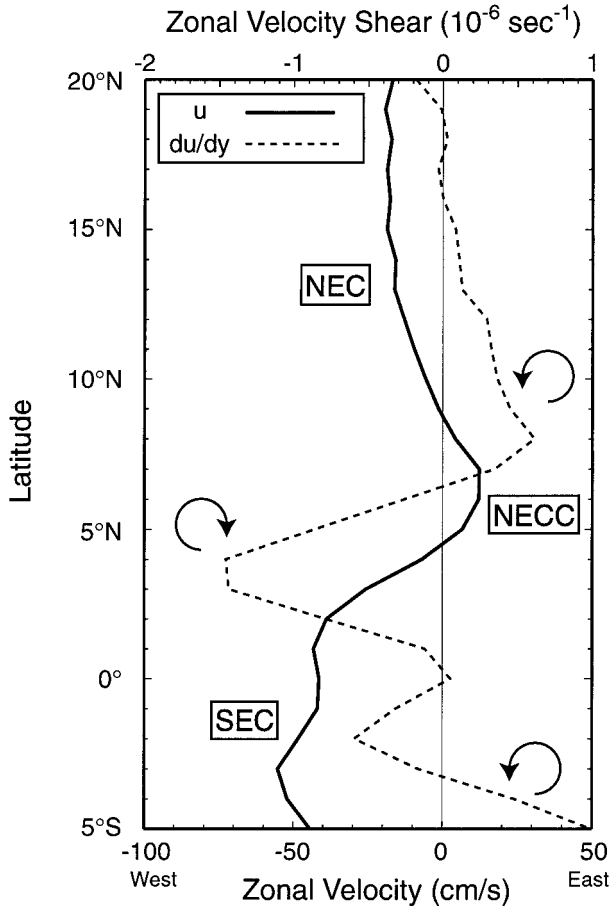

FIG. 12. The meridional variation of zonal velocity in the low-latitude eastern Atlantic Ocean. Curves depict the annual mean, zonally averaged (40°–15°W) zonal velocity (solid: cm s^{-1}) and the meridional gradient of zonal velocity (dashed: 10^{-6} s^{-1}) as a function of latitude. Values were computed from the global ship-drift climatology of Mariano et al. (1995). The approximate location of major zonal currents are indicated. Note in particular the region of positive (cyclonic; anticlockwise) shear between the NECC and the NEC with a maximum near 8°N. This shear is relatively constant in the eastern Atlantic but varies seasonally in the western Atlantic (Richardson and McKee 1984).

surface velocities of 100 cm s^{-1} and R_o exceeding 0.3 (e.g., Olson 1991), the eddy kinetic energy (EKE) associated with this eddy (150 cm^2 s^{-2}) is much greater than the background level calculated from the float trajectory prior to April 1991 (16 cm^2 s^{-2}). For comparison, yearlong moored observations at 8°N in the (very energetic) western tropical Atlantic indicated EKE of 100 cm^2 s^{-2} at 900-m depth (Johns et al. 1990).

A mesoscale eddy free of external influences (i.e., away from topography and excluding large-scale background flows) will self-propagate toward the west due to the change of planetary vorticity with latitude (the β effect; e.g., Cushman-Roisin et al. 1990). A cyclonic eddy will also tend to move poleward, although at a rate much slower than its zonal motion (Chassignet 1989). The translation of the observed eddy was initially northwestward, away from the African coast. In June–July 1991 the direction of motion rotated to a more northward course parallel to the coastline. The large northward component of eddy translation suggests that the observed eddy motion could be due to advection by a background flow rather than by self-propagation. This is consistent with the continued northward motion of float 17 following the cessation of cyclonic looping and provides further evidence for a continuous northward eastern boundary flow at intermediate depths. Though not particularly suggestive of an eastern boundary current, Chepurin and Carton (1997) found hydrographic evidence of relatively broad northward flow at intermediate depths (on the density surface $\sigma_\theta = 27.3$) east of 30°W and extending from the equator to 15°N.

b. Float 19: Loops and large amplitude meanders

Figure 9 shows the path of float 19 between February and October 1990. This trajectory described a series of wavelike meanders superimposed on an eastward flow. The average eastward velocity between June and October was 13.6 cm s^{-1} with maximum eastward velocity exceeding 25 cm s^{-1} in August (Fig. 6). This is comparable to surface velocities associated with the near-surface NECC reported by Richardson and McKee (1984). The NECC, fed from the western boundary by the retroflecting North Brazil Current, accelerates rapidly in May–June in response to the northward migration of the intertropical convergence zone and the resulting increase in the westward trade winds (e.g., Katz 1993). The onset of rapid eastward translation by float 19 was approximately coincident with this seasonal increase in NECC surface velocity. Eastward float velocity decreased from an August maximum to a reversal of direction in November. This is consistent with the observed deceleration of the NECC in the eastern Atlantic (Richardson and Walsh 1986) and in the latter part of the year (Katz 1993; Richardson and McKee 1984). The mean Lagrangian wavelength and period of the meanders were 413 ± 46 km and 35 ± 2 days, based on a sample of seven crest-to-crest measurements. The meanders generally decreased in wavelength and period as the float moved east and its zonal velocity decreased.

Float 19 also performed several cyclonic loops (Fig. 10). However, because the path of eddy translation implied by the trajectory was so erratic, we do not believe the float was trapped within a single coherent eddy. Rather, we speculate that float 19 responded to at least two different recirculations associated with the crests and troughs of the meandering NECC.

6. Discussion

There are several possible explanations for the intermediate-depth mesoscale variability observed in the eastern tropical Atlantic. In this section we consider

whether the observed variability could be the direct subsurface manifestation of surface circulation features such as wind-driven currents, eddies, or waves. There are, of course, other potential mechanisms for generation of middepth variability. Spall (1992) proposed that Rossby waves radiating from the Cape Verde Frontal Zone (Zenk et al. 1991) might generate mesoscale variability at depths of 1000 m in the southeastern North Atlantic. As the intensity of the observed variability was much greater than that predicted by Spall, we find it unlikely that this particular mechanism is dominant.

It is interesting to note that the location of the initial loop of float 17 coincided with the edge of the continental shelf (Figs. 1 and 7). A poleward intermediate-depth eastern boundary current could generate middepth vortices, as in the case of the Mediterranean outflow and the formation of Mediterranean Water eddies near Cape St. Vincent (Bower et al. 1997). However, the eddy formation mechanism invoked by Bower et al. and first described by D'Asaro (1988) preferentially results in the formation of anticyclonic rather than cyclonic vortices. Furthermore, we are not aware of any observations indicating an intermediate-depth eastern boundary current south of 10°N. Nevertheless, the proximity of the first loops of float 17 to the shelf break is striking and leads us to speculate that the abrupt bathymetry may have played a role in the generation of the cyclonic eddy, either directly or indirectly through modification of the surface flow.

Satellite surface temperature observations

To investigate whether surface phenomena might be associated with the intermediate-depth trajectory of float 19, we examined several years of NOAA/NASA Oceans Pathfinder satellite sea surface temperature (SST) data. These data were obtained from the Jet Propulsion Laboratory (JPL) Physical Oceanography Distributed Active Archive Center. Additional information concerning this data product can be found in McClain et al. (1985). To reduce the areal extent of missing data due to cloud cover, SST data were combined to form 10–14-day composite images. Although it introduced some smoothing and spatial distortion, this processing was necessary in order to compensate for the cloudy conditions in the eastern equatorial Atlantic, which severely limited the usefulness of SST imagery for feature identification during boreal summer and fall. Satellite altimetry could have been a useful tool in this investigation but, unfortunately, the time period of interest (mid-1991) falls in a gap between the demise of Geosat and the launch of *ERS-1*.

A 14-day composite image centered on 19 February 1991 (Fig. 11) clearly shows the boundary between relatively warm equatorial water and cooler subtropical gyre water. Note that due to summertime cloudiness in the eastern Atlantic it was not possible to generate a useful composite image coincident in time with the meandering trajectory of float 19. The coldest water in Fig. 11 is located near the eastern boundary and is related to the southward flowing Canary Current and wind-driven upwelling along the African coast (Zenk et al. 1991). Particularly conspicuous is the strong temperature gradient in the eastern Atlantic between 5° and 8°N and the wavelike meridional displacements of this front. The meanders, with crest-to-crest wavelengths of 300–500 km and meridional amplitude of 150–250 km, are comparable in scale to those measured by float 19. A time series of composite images (not shown) indicates that the meander crests near 20°W travel to the west at a rate of about 2° per month, or 8 cm s^{-1}. Using appropriate values for the regional stratification, a first-baroclinic Rossby wave with wavelength 400 km should propagate westward with a phase speed of 7–8 cm s^{-1} (e.g., Pedlosky 1979). Although we lack surface observations truly synoptic with our float measurements, we believe the satellite SST measurements support a hypothesis that the trajectory or float 19 describes the intermediate-depth expression of the meandering near-surface NECC.

Steger and Carton (1991) used satellite-derived SST imagery to determine the characteristics of long waves in the low-latitude Atlantic Ocean. These waves, with a length of about 1000 km and a period near 1 month, are generally referred to as tropical instability waves (e.g., Philander 1976, 1978; Legeckis and Reverdin 1987; Weisberg 1984; Weisberg and Weingartner 1988) and are found within 5° of the equator. Weisberg (1984) found evidence for baroclinic instability as a source of wave energy within the cyclonic shear region on the equator. Weisberg and Weingartner (1988) subsequently clarified that the dominant energy conversion driving the instability was located in the cyclonic shear region of the SEC.

The cyclonic looping and frequent direction changes of float 19 (Fig. 10) are suggestive of a response to shear along the northern edge of the NECC (i.e., at the boundary between the NECC and the NEC rather than the SEC). Given the observed differences in zonal wavelength (400 vs 1000 km) and meridional location, we speculate that tropical instability waves as previously described are not directly responsible for the observed meandering of float 19, but that a similar physical mechanism (namely horizontal shear) may be important in generating meanders along the boundary between the NECC and NEC. The global shipdrift climatology of Mariano et al. (1995) confirms the existence of a significant region of anticlockwise (cyclonic) upper-ocean shear in this region (Fig. 12). The core of the NECC is located near 6°N in the eastern Atlantic, while the cyclonic shear between the NECC and NEC is greatest near 8°N.

The meanders in the eastern Atlantic were observed to be quite steep and to occasionally break, forming extended filaments of warm equatorial water interleaved with cooler subtropical gyre water. A particularly clear

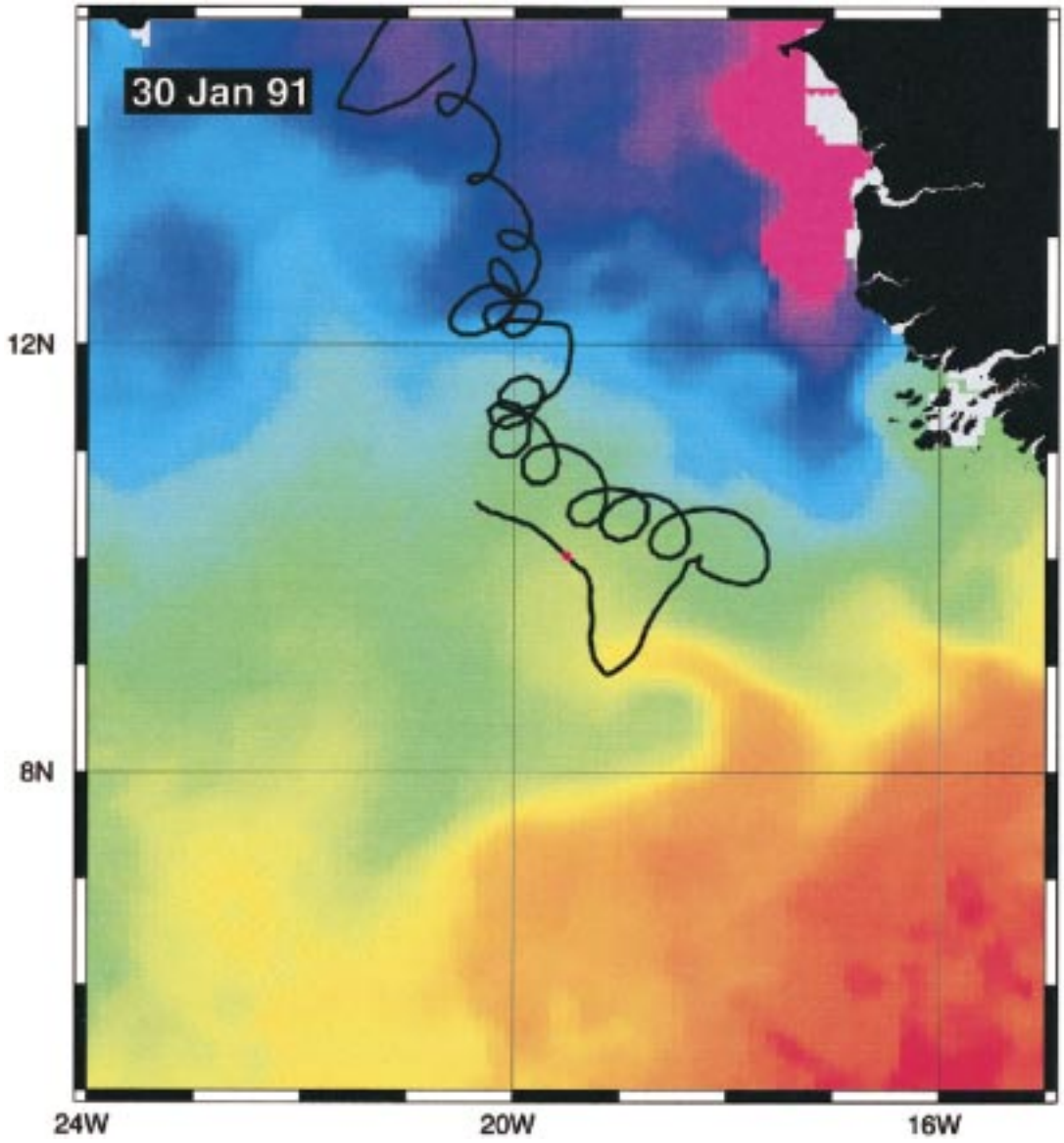

FIG. 13. Fourteen-day composite sea surface temperature image centered on 30 January 1991 in the eastern tropical Atlantic. The cold core, cyclonic recirculation near 8.5°N, 19.7°W within the crest of a breaking wave is approximately 100 km in diameter. The trajectory of float 17 during 1991 is shown. The location of the float on the date corresponding to the image is indicated by the red dot. The wave crests in this figure subsequently moved westward at about 8 cm s^{-1}. The color palette is the same as that used in Fig. 11.

example of this is shown in Fig. 13. These billows and breaking waves are indicative of horizontal shear along the interface between the warm, eastward flowing NECC and the cooler, westward flowing NEC. As mentioned above, we speculate that the loops exhibited by float 19 (Fig. 10) were caused by the circulation associated with passing or breaking meander crests. Specifically, we believe float 19 began moving eastward in the NECC, was entrained within a meander, and then carried northward into the westward flowing NEC. While traveling in the NEC, the float was repeatedly captured and ejected by meander-related recirculations near the boundary between eastward and westward flow.

A breaking meander, such as in Fig. 13, could have generated the intense cyclonic eddy that trapped float 17. If this eddy were the intermediate-depth manifestation of a surface feature, one might expect to find a translating SST anomaly consistent with the horizontal scale and trajectory of the observed eddy. We searched for such an anomaly in a series of composite images and in individual (unsmoothed) satellite passes, but were unsuccessful. We conclude that if a closed surface cir-

culation feature were associated with the intermediate-depth eddy, any related SST signature was masked by local surface heating.

7. Summary and conclusions

New Lagrangian observations of the subsurface circulation in the low-latitude eastern Atlantic were presented. These observations suggest the existence of an intermediate-depth eastern boundary current along the northwest coast of Africa and a potential pathway for the northward intergyre transport of intermediate water. The float trajectories also illustrate energetic eddies and meanders at depths of 1000 m. Satellite SST imagery revealed that the large amplitude intermediate-depth meanders measured by the floats are comparable to those of the eastward flowing NECC, and horizontal shear between the opposing NEC and NECC was suggested as a mechanism responsible for the generation of these meanders. An intense (EKE ten times background levels) and persistent (5 months) cyclonic eddy near the eastern boundary was identified, and its rotational and translational characteristics were determined. Large-amplitude breaking current meanders seen in satellite imagery were hypothesized as a possible mechanism for the generation of this eddy. Abrupt bathymetry near the continental shelf break was also considered as potentially relevant to the formation of the eddy. Further investigation, including perhaps the examination of synthetic Lagrangian floats in numerical ocean models, could be helpful in determining the relative importance of these mechanisms.

Our present understanding of intermediate-depth currents near the tropical eastern boundary is quite poor. Additional surface and subsurface measurements (both Lagrangian and Eulerian) near the African coast are necessary to confirm our observation of an intermediate-depth eastern boundary current. These measurements could clarify the relationship between surface and intermediate-depth circulation in the eastern Atlantic and would lead to an improved general understanding of the characteristics and causes of subsurface variability.

Acknowledgments. Support for the authors during preparation of this manuscript was provided by the National Science Foundation through Grant OCE91-14656. The SOFAR float observations were supported by NSF through Grants OCE85-17375 and OCE85-21082 to W. J. Schmitz and P. L. Richardson. The float trajectories were processed by Marg Zemanovic and Chris Wooding. We thank Ed Ryan and Arthur Mariano for sharing data and figures from their global shipdrift climatology. The comments and suggestions of Larry Pratt and two anonymous reviewers helped focus and improve this manuscript.

REFERENCES

Barton, E. D., 1989: The poleward undercurrent on the eastern boundary of the subtropical North Atlantic. *Poleward Flows Along Ocean Boundaries,* S. J. Neshyba et al., Eds., Springer-Verlag, 82–95.

Bower, A. S., L. Armi, and I. Ambar, 1997: Lagrangian observations of Meddy formation during a Mediterranean undercurrent seeding experiment. *J. Phys. Oceanogr.,* **27,** 2545–2575.

Chassignet, E. P., 1989: On the meridional propagation of isolated eddies: 1989 summer study program in geophysical fluid dynamics. Tech. Rep. WHOI-89-54, Woods Hole Oceanographic Institution, Woods Hole, MA, 35 pp. [Available from Woods Hole Oceanographic Institution, Woods Hole, MA 02543.]

Chepurin, G., and J. A. Carton, 1997: The hydrography and circulation of the upper 1200 meters in the tropical North Atlantic during 1982–1991. *J. Mar. Res.,* **55,** 633–670.

Cushman-Roisin, B., E. P. Chassignet, and B. Tang, 1990: Westward motion of mesoscale eddies. *J. Phys. Oceanogr.,* **20,** 758–768.

D'Asaro, E. A., 1988: Generation of submesoscale vortices: A new mechanism. *J. Geophys. Res.,* **93,** 6685–6693.

Düing, W., F. Ostapoff, and J. Merle, 1980: *Physical Oceanography of the Tropical Atlantic during GATE.* University of Miami, 117 pp.

Fratantoni, D. M., 1996: On the pathways and mechanisms of upper-ocean mass transport in the tropical Atlantic Ocean. University of Miami/RSMAS Tech. Rep. RSMAS-96-006, 250 pp. [Available from University of Miami/RSMAS, 4600 Rickenbacker Causeway, Miami, FL 33149.]

——, W. E. Johns, and T. L. Townsend, 1995: Rings of the North Brazil Current: Their structure and behavior inferred from observations and a numerical simulation. *J. Geophys. Res.,* **100,** 10 633–10 654.

Garzoli, S. L., and E. J. Katz, 1983: The forced annual reversal of the Atlantic North Equatorial Countercurrent. *J. Phys. Oceanogr.,* **13,** 2082–2106.

Johns, W. E., T. N. Lee, F. A. Schott, R. J. Zantopp, and R. H. Evans, 1990: The North Brazil Current retroflection: Seasonal structure and eddy variability. *J. Geophys. Res.,* **95,** 22 103–22 120.

Katz, E. J., 1993: An interannual study of the Atlantic North Equatorial Countercurrent. *J. Phys. Oceanogr.,* **23,** 116–123.

Legeckis, R., and G. Reverdin, 1987: Long waves in the equatorial Atlantic during 1983. *J. Geophys. Res.,* **92,** 2835–2842.

Mariano, A. H., E. H. Ryan, B. D. Perkins, and S. Smithers, 1995: The Mariano Global Surface Velocity Analysis 1.0. U.S. Coast Guard Rep. No. CG-D-34-95, 55 pp. [Available from University of Miami/RSMAS, 4600 Rickenbacker Causeway, Miami, FL 33149.]

Mayer, D. A., and R. H. Weisberg, 1993: A description of COADS surface meteorological fields and the implied Sverdrup transports for the Atlantic Ocean from 30°S to 60°N. *J. Phys. Oceanogr.,* **23,** 2201–2221.

McClain, E. P., W. Pichel, and C. Walton, 1985: Comparative performance of AVHRR-based multichannel sea surface temperatures. *J. Geophys. Res.,* **90,** 11 587–11 601.

Olson, D. B., 1991: Rings in the ocean. *Ann. Rev. Earth Planet. Sci.,* **19,** 283–311.

Pedlosky, J., 1979: *Geophysical Fluid Dynamics.* Springer-Verlag, 625 pp.

Philander, S. G. H., 1976: Instabilities of zonal equatorial currents. *J. Geophys. Res.,* **81,** 3725–3735.

——, 1978: Instabilities of zonal equatorial currents 2. *J. Geophys. Res.,* **83,** 3679–3682.

Reid, J. L., 1994: On the total geostrophic circulation of the North Atlantic Ocean: Flow patterns, tracers, and transports. *Progress in Oceanography,* Vol. 33, Pergamon, 1–92.

Richardson, P. L., 1984: Drifting buoy trajectories in the Atlantic North Equatorial Countercurrent during 1983. *Geophys. Res. Lett.,* **11,** 745–748.

——, and T. K. McKee, 1984: Average seasonal variation of the

Atlantic equatorial currents from historical ship drifts. *J. Phys. Oceanogr.*, **14,** 1226–1238.

——, and D. Walsh, 1986: Mapping climatological seasonal variations of surface currents in the tropical Atlantic using ship drifts. *J. Geophys. Res.*, **91,** 10 537–10 550.

——, and W. J. Schmitz Jr., 1993: Deep cross-equatorial flow in the Atlantic measured with SOFAR floats. *J. Geophys. Res.*, **98,** 8371–8387.

——, and D. M. Fratantoni, 1999: Float trajectories in the deep western boundary current and deep equatorial jets of the tropical Atlantic. *Deep-Sea Res.*, in press.

——, M. E. Zemanovic, C. M. Wooding, W. J. Schmitz, and J. F. Price, 1992: SOFAR float trajectories from an experiment to measure the Atlantic cross-equatorial flow (1989–1990). Tech. Rep. WHOI-92-33, Woods Hole Oceanographic Institution, Woods Hole, MA, 187 pp. [Available from Woods Hole Oceanographic Institution, Woods Hole, MA 02543.]

——, ——, ——, and ——, 1994a: SOFAR float trajectories in the tropical Atlantic 1989–1992. Tech. Rep. WHOI-94-33, Woods Hole Oceanographic Institution, Woods Hole, MA, 185 pp. [Available from Woods Hole Oceanographic Institution, Woods Hole, MA 02543.]

——, G. E. Hufford, R. Limeburner, and W. S. Brown, 1994b: North Brazil Current retroflection eddies. *J. Geophys. Res.*, **99,** 5081–5093.

Schmitz, W. J., 1995: On the interbasin-scale thermohaline circulation. *Rev. Geophys.*, **33,** 151–173.

Spall, M. A., 1992: Rossby wave radiation in the Cape Verde frontal zone. *J. Phys. Oceanogr.*, **22,** 796–807.

Steger, J. M., and J. A. Carton, 1991: Long waves and eddies in the tropical Atlantic Ocean: 1984–1990. *J. Geophys. Res.*, **96,** 15 161–15 172.

Weisberg, R. H., 1984: Instability waves on the equator in the Atlantic Ocean during 1983. *Geophys. Res. Lett.*, **11,** 753–756.

——, and T. J. Weingartner, 1988: Instability waves in the equatorial Atlantic Ocean. *J. Phys. Oceanogr.*, **18,** 1641–1657.

Zenk, W., B. Klein, and M. Schroder, 1991: Cape Verde Frontal Zone. *Deep-Sea Res.*, **38,** 505–530.